Observation of the controlled assembly of preclick components in the in situ click chemistry generation of a chitinase inhibitor

Tomoyasu Hirose[a,1], Nobuo Maita[b,1], Hiroaki Gouda[c,1], Jun Koseki[c], Tsuyoshi Yamamoto[a], Akihiro Sugawara[a], Hirofumi Nakano[a], Shuichi Hirono[c], Kazuro Shiomi[a], Takeshi Watanabe[d], Hisaaki Taniguchi[b], K. Barry Sharpless[e,f], Satoshi Ōmura[a,2], and Toshiaki Sunazuka[a,2]

[a]The Kitasato Institute, Kitasato Institute for Life Sciences and Graduate School of Infection Control Sciences, and [c]School of Pharmacy, Kitasato University, Tokyo 108-8641, Japan; [b]Institute for Enzyme Research, The University of Tokushima, Tokushima City, Tokushima 770-8503, Japan; [d]Department of Applied Biological Chemistry, Faculty of Agriculture, Niigata University, Niigata 950-2181, Japan; and [e]Department of Chemistry and [f]The Skaggs Institute for Chemical Biology, The Scripps Research Institute, La Jolla, CA 92037

Contributed by Satoshi Ōmura, August 21, 2013 (sent for review March 4, 2013)

The Huisgen cycloaddition of azides and alkynes, accelerated by target biomolecules, termed "in situ click chemistry," has been successfully exploited to discover highly potent enzyme inhibitors. We have previously reported a specific *Serratia marcescens* chitinase B (*Sm*ChiB)-templated *syn*-triazole inhibitor generated in situ from an azide-bearing inhibitor and an alkyne fragment. Several in situ click chemistry studies have been reported. Although some mechanistic evidence has been obtained, such as X-ray analysis of [protein]–["click ligand"] complexes, indicating that proteins act as both mold and template between unique pairs of azide and alkyne fragments, to date, observations have been based solely on "postclick" structural information. Here, we describe crystal structures of *Sm*ChiB complexed with an azide ligand and an *O*-allyl oxime fragment as a mimic of a click partner, revealing a mechanism for accelerating *syn*-triazole formation, which allows generation of its own distinct inhibitor. We have also performed density functional theory calculations based on the X-ray structure to explore the acceleration of the Huisgen cycloaddition by *Sm*ChiB. The density functional theory calculations reasonably support that *Sm*ChiB plays a role by the cage effect during the pretranslation and posttranslation states of selective *syn*-triazole click formation.

argifin | target-guided synthesis | cocrystal structure | molding effect

The Huisgen cycloaddition of azides and alkynes is a pure [2+3] thermal dipolar cycloaddition reaction (1), which becomes nonconcerted when the reaction is catalyzed by Cu(I) (2, 3). This provides ready access to 1,4-disubstituted 1,2,3-triazles and is one of the most commonly recognized reactions of "click chemistry" (3). Since 2002, several studies of click chemistry applying Cu(I)-catalyzed 1,2,3-triazle formation have been published and it has now been used in many areas of research. "In situ click chemistry" represents a target-guided synthesis technique for discovering protein ligands. It is dependent on Huisgen cycloaddition reactions between azide and alkyne reagents that are inert under physiological conditions, where metal catalysts such as Cu(I) (4) are absent. During the past decade, in situ click chemistry approaches, based on the use of proteins as templates to covalently assemble fragments by Huisgen cycloaddition, have been increasingly successfully demonstrated (5–16). In our strategy, we used chitinases from *Serratia marcescens* (*Sm*Chi) as target template enzymes for in situ click chemistry study.

Chitinases are enzymes that hydrolyze chitin, a homopolymer of β-(1,4)-linked *N*-acetylglucosamine, which is the second most abundant polysaccharide in nature, being the major structural constituent of fungal cell walls, the shells of crustaceans and arthropods, and the microfilarial sheaths of parasitic nematodes (17–19). Chitinases are present in a wide variety of organisms, ranging from bacteria to animals, and their biological roles vary depending on the function of chitin among different species (20–22). Chitinases are currently classified into two different families of glycosyl hydrolases, namely family 18 and family 19, on the basis of amino acid sequence similarities (23, 24). Recently, family-18 chitinases have become attractive as targets for possible treatments for certain human infectious and inflammatory diseases. For example, onchocerciasis, commonly known as river blindness, is a neglected tropical disease caused by infection with the filarial nematode, *Onchocerca volvulus*. Janda and his coworkers identified closantel, a veterinary anthelmintic with known proton ionophore activities, as a potent and specific inhibitor of filarial chitinases (classified into family 18), which can completely prevent L3 to L4 stage molting of *O. volvulus* larvae (25). So far, many inhibitors of the family-18 chitinases have been reported, offering the promise for development of new therapeutic agents against chitinase-connected infectious diseases and chitinase-mediated pathologies. During screening of over 10,000 extracts from soil microorganisms, our research group has discovered naturally occurring cyclic pentapeptide chitinase inhibitors, argadin (26) and argifin (**1**) (27–29). In 2009, we reported the design of an azide-bearing N^{ω}-methylcarbamoyl-L-arginine substrate (**2**), a simpler derivative of **1**, and the

Significance

Several in situ click chemistry studies have been reported. To date, there is evidence to indicate that proteins act as mold between azide and alkyne fragments by X-ray analysis of protein–ligand complexes. However, only "postclick" structural evidence has been available. We succeeded in obtaining crystal structures of a chitinase complexed with an azide inhibitor and an *O*-allyl oxime fragment as a mimic of a click partner, revealing a mechanism for accelerating triazole formation in chitinase. This is an example to express the "preclick" state of in situ click chemistry and a demonstration to show that the in situ click chemistry approach will benefit from this analysis for future plans. We also performed density functional theory calculations to explore the chitinase-contributed Huisgen cycloaddition.

Author contributions: T.H., S.Ō., and T.S. designed research; T.H., N.M., T.Y., and A.S. performed research; H.N., K.S., T.W., H.T., and K.B.S. contributed new reagents/analytic tools; H.G., J.K., and S.H. analyzed data; and T.H., N.M., and H.G. wrote the paper.

The authors declare no conflict of interest.

Data deposition: The atomic coordinates and structure factors have been deposited in the Protein Data Bank, www.pdb.org (PDB ID codes 3WD0, 3WD1, 3WD2, 3WD3, and 3WD4).

[1]T.H., N.M., and H.G. contributed equally to this work.

[2]To whom correspondence may be addressed. E-mail: omuras@insti.kitasato-u.ac.jp or sunazuka@lisci.kitasato-u.ac.jp.

This article contains supporting information online at www.pnas.org/lookup/suppl/doi:10.1073/pnas.1315049110/-/DCSupplemental.

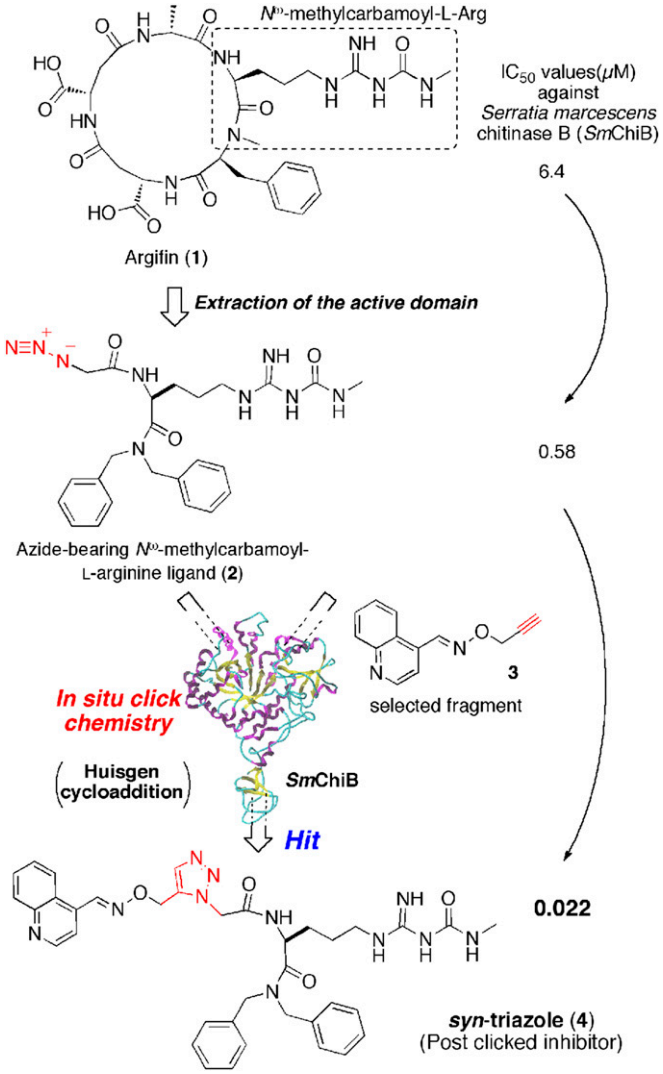

Fig. 1. Our previous result for in situ click chemistry. A bacterial chitinase [*Serratia marcescens* chitinase B (*Sm*ChiB)] guided the formation of a more potent *syn*-triazole obstructer (**4**) involved in chitin hydrolysis via in situ click chemistry between the active azide ligand (**2**), simplified from natural product argifin (**1**), and an alkyne fragment (**3**).

application of in situ click chemistry for the generation of more potent chitinase inhibitors (11) (Fig. 1). Information about binding of chitin substrates and some inhibitors including **1** [IC_{50} = 6.4 μM against *S. marcescens* chitinase B (*Sm*ChiB)] in the tunnel-like active site, and the chitin hydrolytic mechanism of *Sm*Chi based on X-ray crystallography are easily available (30–33). In fact, *Sm*ChiB itself serves as a mold to enable production of the *syn*-triazole (**4**) from **2** (IC_{50} = 0.58 μM) with quinoline-oxime (**3**) (IC_{50} = >100 μM), found from a library of 71 randomly collected, structurally diverse alkynes, via the enzyme template Huisgen cycloaddition process. *Syn*-triazole **4** (IC_{50} = 0.022 μM) demonstrated heightened potency with IC_{50} values against *Sm*ChiB smaller than the precursor (**2**) as well as the natural product argifin (**1**). In contrast, the *anti*-triazole isomer of **4**, not formed in *Sm*ChiB, exhibited only comparatively moderate inhibition (IC_{50} = 1.0 μM) (11). In the process of in situ click chemistry, the highly exergonic nature of triazole formation is irreversible and thereby locks in unique characteristics. In previous in situ click chemistry studies, some triazole compounds have been cocrystallized with corresponding target proteins to investigate hypotheses about specific interactions where the target enzymes can serve as atomic-scale reaction molds to create their own inhibitors (14, 16, 34). However, direct observations of the controlled assembly of in situ click chemistry candidates in target enzymes have not been reported to date. Thus, the structural analysis of in situ click chemistry candidates in the target enzyme by X-ray crystallography may shed light on the kinetically controlled in situ phenomenon.

We have determined the crystal structures of complexes of *Sm*ChiB with azide ligand (**2**) (click precursor) and *syn*-triazole (**4**) (generated in situ), together with the three-component complex of [*Sm*ChiB]–[**2**]–[mimic of alkyne-bearing quinoline-oxime fragment], respectively. Subsequently, the crystal structure of the three-component complex was remodeled to [*Sm*ChiB]–[**2**]–[**3**], as an assembly of in situ click chemistry candidates, based on a detailed analysis of the crystal structures with in silico calculation. The complex of [*Sm*ChiB]–[**2**]–[**3**] was analyzed by density

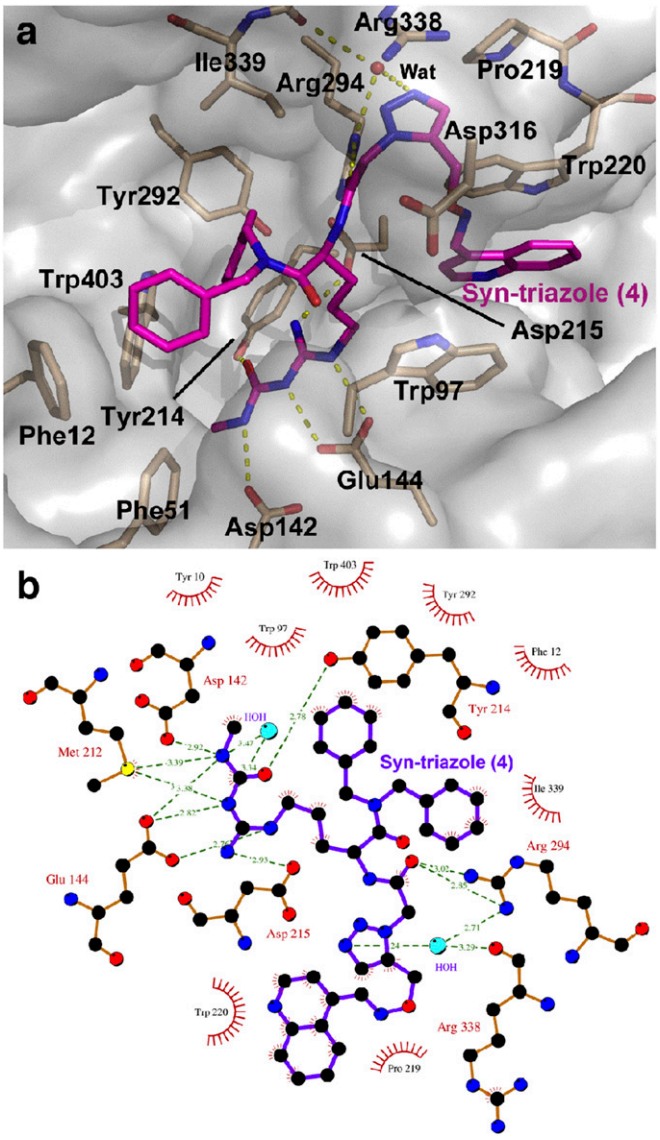

Fig. 2. *Syn*-triazole (**4**) (postclicked inhibitor) complexed to *Sm*ChiB. (*A*) The surface representation of *Sm*ChiB with a postclicked inhibitor **4** colored magenta and interacting residues colored light brown are shown as stick model (blue, nitrogens; red, oxygens). (*B*) Schematic drawing of the detailed interactions between *Sm*ChiB and **4** (blue, nitrogens; red, oxygens; black, carbons).

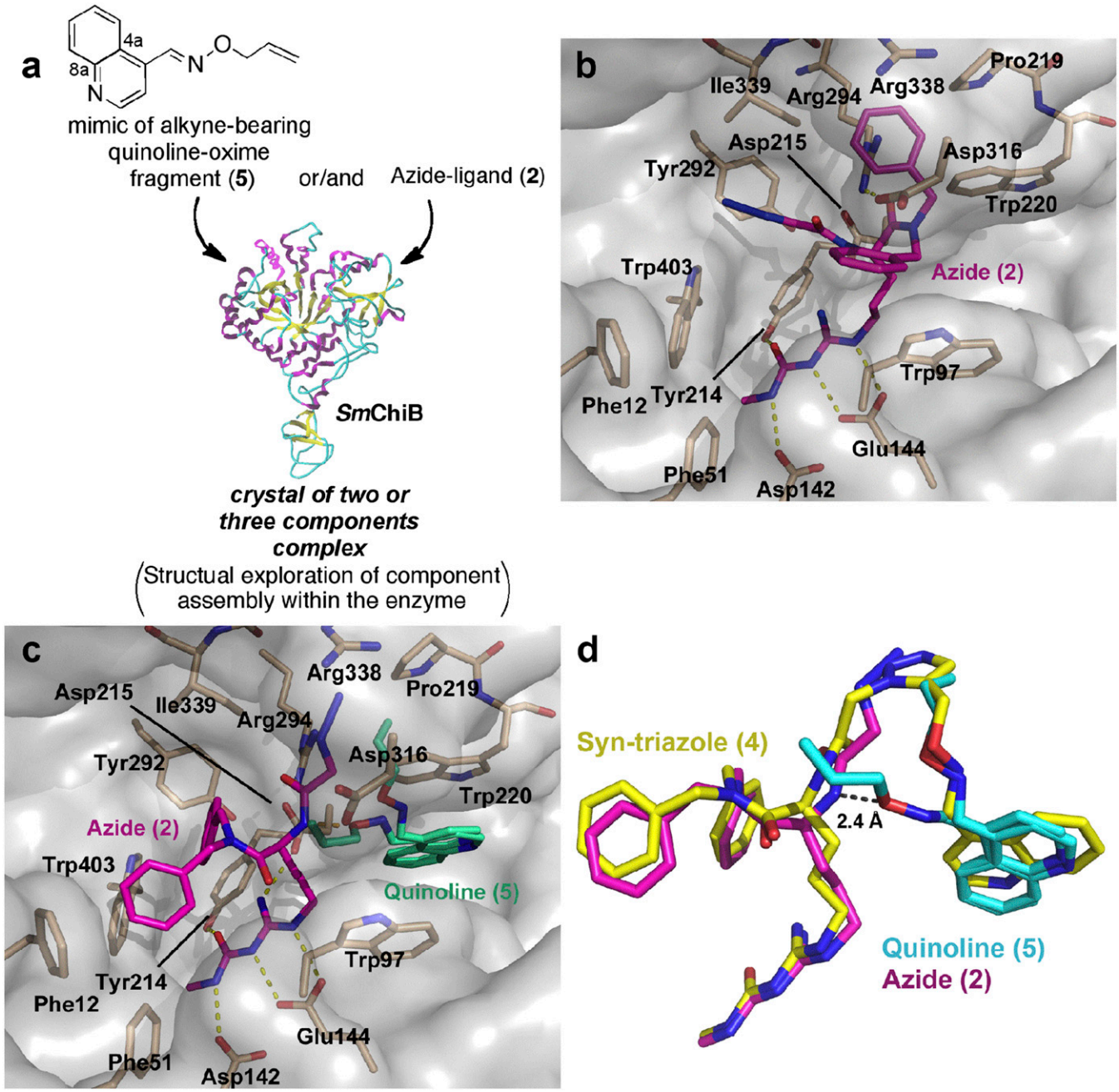

Fig. 3. Visualization of the intermediates in triazole formation. (*A*) Preparation of *Sm*ChiB complex with azide ligand (**2**) or/and quinoline fragment (**5**) as a mimic of alkyne fragment (**3**) to indicate the state before in situ triazole formation between **2** and **3** in *Sm*ChiB. (*B*) An azide ligand (**2**) complexed to *Sm*ChiB (colored as in Fig. 2*A*). (*C*) Both azide ligand (**2**) and quinoline fragment (**5**) (green) complexed to *Sm*ChiB (colored as in Fig. 2*A*). (*D*) *Syn*-triazole (**4**) (yellow) is superimposed on the azide ligand (**2**) (magenta) and quinoline fragment (**5**) (light blue).

functional theory (DFT) calculations to explore the *Sm*ChiB-induced Huisgen cycloaddition. The DFT calculation suggests that the activation barrier of triazole formation in the solvent (H_2O) was approximately equal with that in the protein. This means that the enzyme works by guiding the assembly of the click candidates. The DFT calculation reasonably supports the theory that *Sm*ChiB plays a role via the cage effect, not as a catalyst, during the pretransition states of triazole formation, and that molecules of **2** and **3** are potentially coupled to generate only **4** among two possible cycloaddition patterns (*syn* and *anti*) by conformational selection in the active site of *Sm*ChiB.

Results and Discussion

Preparation of the *Sm*ChiB Complexes and Structural Analysis of in Situ Click Chemistry. To understand how *Sm*ChiB recognizes the *syn*-triazole (**4**) at the atomic level, we determined the crystal structures of *Sm*ChiB alone and after soaking with **4** at 1.7- and 2.3-Å resolution, respectively (*Materials and Methods*) (Fig. 2). The *N*-methylcarbamoyl-L-arginine moiety of **4** is, as expected, bound at the active site of *Sm*ChiB with the same orientation as argifin (**1**) (31). In addition, the dibenzyl moiety of **4** is embedded in the hydrophobic region of the binding cleft composed of Phe12, Phe51, Tyr292, Ile339, and Trp403. The triazole of **4**, as a bridging function between the azide ligand (**2**) and quinoline-

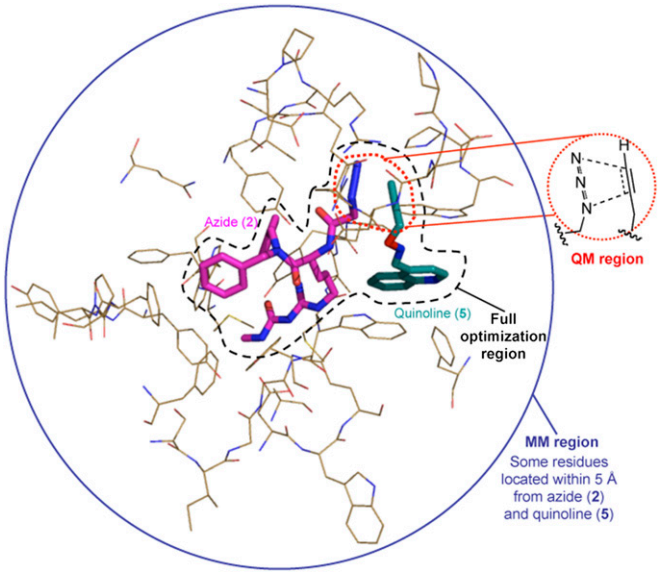

Fig. 4. The quantum mechanics (QM) and molecular mechanics (MM) regions in ONIOM calculations. Compounds **2** and **3** were fully optimized in all our calculations, whereas the total of 39 *Sm*ChiB residues, i.e., Tyr10, Tyr11, Phe12, Ile13, Pro14, Phe51, Ser93, Ile94, Gly95, Gly96, Trp97, Tyr98, Asp142, Trp143, Glu144, Ala184, Phe191, Met212, Thr213, Tyr214, Asp215, Pro219, Trp220, Tyr292, Gly293, Arg294, Pro313, Gly314, Glu315, Asp316, Pro317, Asp336, Pro337, Arg338, Ile339, Met401, Phe402, Trp403, and Gln407, were restricted to each initial coordinate during ONIOM optimization (colored as in Fig. 3*C*).

oxime (**3**), is fitted within the pocket composed of Pro219, Arg294, Asp336, Arg338, and Ile339. The quinoline moiety of **4** is sandwiched by two tryptophan residues of Trp97 and Trp220, presumably with strong π–π interaction.

We subsequently attempted to visualize the assemblage of each click candidate for the pretriazole formation (Fig. 3*A*). For this, we hypothesized that, if the alkyne substrate (**3**) is located and stabilized in appropriate orientations with the azide ligand (**2**) by the molding effect of *Sm*ChiB, it is likely that the reaction components would combine within the crystal to generate a high-affinity substrate (**4**), thus preventing the recording of a high-resolution snapshot of the complex by X-ray crystallography. Therefore, we prepared the alkyne mimic compound (**5**) (IC_{50} = > 100 μM) (*SI Materials and Methods*, Figs. S1–S4), which has a double bond instead of a terminal alkyne. First, **5** alone was soaked into *Sm*ChiB crystals at high concentration (1.25 mM in crystallization droplet). However, no distinct electron density was observed. Next, the azide ligand (**2**) was cocrystallized with *Sm*ChiB to see how **2** alone binds to *Sm*ChiB. Interestingly, the head region of the azide ligand (**2**) was rotated about 180° compared with the *syn*-triazole (**4**) orientation (Fig. 3*B*). The crystallographic B factor of the head region was much higher than the *N*-methylcarbamoyl-L-arginine moiety. This indicates that the head region is loosely bonded, whereas the *N*-methylcarbamoyl-L-arginine portion tightly binds to *Sm*ChiB. The soaking of azide ligand (**2**) and alkyne mimic compound (**5**) together with the *Sm*ChiB crystals at lower concentration (12.5 μM of **2** and 125 μM of **5**) revealed only the electron density from **2**, with the same orientation as **2** alone. When increasing the concentration of the compounds (250 μM of **2** and 1.25 mM of **5**), the electron densities of both compounds appeared. The azide ligand (**2**) could be fitted to the electron density of the same orientation as the *syn*-triazole (**4**). In addition, the residual electron density resembled a two-horned goat head, which presumably results in the two conformers of **5** (Fig. 3*C* and Fig. S5). Both conformers were stacked between Trp97 and Trp220, as seen in *syn*-triazole (**4**), but the quinolone ring of **5** was flipped about a half-turn from the stacking mode of the quinolone moiety of **4** on the bond between C-4a and C-8a. As the participation of the nitrogen atoms in the quinolone ring of **4** and **5** were not observed in the interaction with the amino acid residues of *Sm*ChiB, it can be expected that there is no variance for binding affinities caused by reorientation of the quinolone ring. The oxygen atom of one conformer of **5** formed a hydrogen bond with the nitrogen atom of azideacetyl amide in the azide ligand (**2**). Orientation of another conformer well overlapped with the *syn*-triazole (**4**) (Fig. 3*D*), representing an assemblage of each click candidate in the reaction.

DFT Calculations Based on X-Ray Cocrystal Structure. To explore how *Sm*ChiB contributes to the Huisgen cycloaddition, we performed DFT calculations. We first modeled the complex structure of [*Sm*ChiB]–[azide ligand (**2**)]–[alkyne fragment (**3**)] using the crystal structure of [*Sm*ChiB]–[**2**]–[mimic of alkyne fragment (**5**)], and performed energy minimization with the AMBER force field to relax the model structure (35, 36). We then constructed the system for the geometry optimization using the ONIOM method (37, 38), which consisted of **2**, **3**, and a total of 39 residues of *Sm*ChiB located within 5 Å from these two compounds. The quantum mechanics (QM) and molecular mechanics (MM) regions in the ONIOM calculation are illustrated in Fig. 4. We defined "the azide and the contiguous methylene group of **2**" and "propargyl group of **3**" as a high-level layer with DFT (B3LYP functional), using a 6-31G* Gaussian basis set, and the remaining atoms of **2**, **3**, and *Sm*ChiB residues as a low-level layer with the AMBER force field (36). The coordinates of *Sm*ChiB residues were constrained to those of the initial structure. We performed ONIOM optimization for three kinds of forms, i.e., precursor state complex, transition state (TS) complex, and product complex, followed by one-point B3LYP calculations using the 6-31G* basis set to estimate the Huisgen cycloaddition barrier in *Sm*ChiB.

Fig. 5 shows the relative energies of the precursor state, TS state, and product complex with B3LYP calculations using the 6-31G* basis set, and the optimized coordinates around the center of Huisgen cycloaddition, based on the ONIOM (B3LYP/6-31G*:AMBER) method for each complex. The relative energies were defined as the deviation energy from the precursor state complex. Our TS complex, optimized under the protein environment, was found to be very similar to that reported for the cycloaddition of methyl azide and propyne in the COSMO

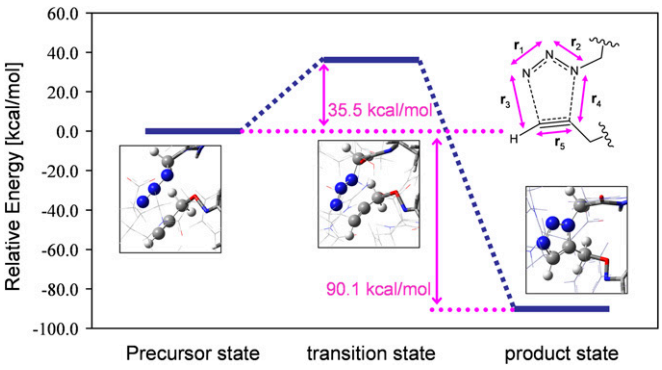

Fig. 5. Relative energies of the reaction via the enzyme complex: precursor state, transition state (TS), and product state with B3LYP calculations using 6-31G* basis set, and the coordinate around the center of Huisgen cycloaddition for each form. The relative energies were defined as deviation energy from the energy for the precursor state.

Table 1. Optimized distances between neighboring heavy atoms in transition-state (TS) complex: The definitions of the lengths are shown in Fig. 5

Positions between azide and alkyne	r_1 (N=N)	r_2 (N=N)	r_3 (N...C)	r_4 (N...C)	r_5 (C≡C)
Protein environment (our result)	1.18	1.23	2.17	2.22	1.23
COSMO implicit solvent (previous work*)	1.17	1.26	2.08	2.24	1.23

Values are in angstroms.

*TS structure for the cycloaddition reaction of methyl azide and propyne in the COSMO implicit solvent model (39).

implicit solvent model (39). As shown in Table 1, there is not much difference in the heavy-atom distance between the in-protein environment and in the COSMO implicit solvent model. This indicated that the protein environment might not have significant influence on the TS structure. The relative energy between the precursor state and TS complex, i.e., the activation barrier, was estimated to be 35.5 kcal/mol, which was somewhat higher than a value of 26.0 kcal/mol reported in the COSMO implicit solvent model (39). In terms of the contribution of water, we performed additional DFT (using B3LYP functional) calculations using a system in gas phase and in water phase with the polarizable continuum model. From these calculations, the difference of the reaction barrier between these phases is less than 3.5 kcal/mol, indicating that the effect of water for this triazole formation might not be significant. In our calculations, zero point energy correction and thermodynamic effect were not included because of the large size of system and the strict shortage of our computational resource. Therefore, the reaction barrier might be overestimated to some extent. Nevertheless, our result suggested that the activation barrier of the protein environment might be higher than that of aqueous environment. However, we could successfully obtain the product compound by triazole formation using *Sm*ChiB. In this respect, we considered that complexation of compounds **2** and **3** by the protein causes a loss of degrees of freedom, which results in a higher frequency of collision between the two reactants. These observations and considerations suggest that *Sm*ChiB mainly plays a role through a cage effect, which leads to an increased frequency of collision between **2** and **3** in favorable orientation, which causes an acceleration of the Huisgen cycloaddition in *Sm*ChiB. The heat of reaction of –90.1 kcal/mol indicated that the product molecule was very stable, and the reaction is, in general, irreversible.

Conclusions

Currently, there is no definitive evidence to support the theory that proteins act as both mold and template between a unique pair of azide and alkyne fragments for in situ click chemistry studies. Our results demonstrate that the assembly of azide ligand (**2**) and alkyne-bearing quinolone-oxime (**3**) within *Sm*ChiB is responsible for yielding a very potent *syn*-triazole inhibitor (**4**) via an in situ click chemistry reaction, as visualized by X-ray crystallography. Moreover, computed analysis of the complex of [*Sm*ChiB]–[**2**]–[**3**], which was remodeled from cocrystal of [*Sm*ChiB]–[**2**]–[mimic of alkyne fragment **3** (**5**)], further supports the favorable orientation for *syn* selective Huisgen cycloaddition by the cage effect of *Sm*ChiB, meaning a reduction in the degrees of freedom of **2** and **3** in enzyme, which causes a higher frequency of reactants hitting each other. Conformation of the [*Sm*ChiB]–[**2**]–[**3**] and [*Sm*ChiB]–[**2**] complexes are different due to the inherent flexibility of both the arginine-based inhibitor and *Sm*ChiB molecules. Therefore, the structures of the precursor complex [*Sm*ChiB]–[**2**] and the product complex [*Sm*ChiB]–[*syn*-triazole (**4**)] alone do not explain the effect of the mysterious acceleration of its *syn*-triazole formation. Our observation suggests that the complex of [enzyme]–[ligand] may be very flexible and reoriented by the coordination of another fragment around the affinity site of the ligand. Consequently, the conformation of the ligand in the complex is changed to a metastable state from the stable conformation, which, in the case of in situ click chemistry, leads to the generation of its own inhibitor. The flexibility of the ligand binding pocket of the protein provides an opportunity to explore a diversity of ligands. However, even if the structural information for the apoenzyme and [target enzyme]–[ligand] complexes could be determined, the prediction of in situ click chemistry candidates is not straightforward, due to the inherent flexibility of proteins and ligands and their ability to spontaneously adopt multiple conformations relative to each other.

Materials and Methods

Expression, Purification, and Crystallization of *Sm*ChiB. The hexahistidine-tagged *Sm*ChiB was expressed and purified as described previously (11). The hexahistidine-tag was removed by adding enterokinase (EKMax; Invitrogen) at 288 K for two overnight periods, and then loaded onto a gel filtration column (Superdex 200 10/300; GE Healthcare) equalized with buffer A (25 mM Tris·Cl, pH 7.5, 0.1 M NaCl). To remove the uncleaved polypeptides, a nickel column (HisTrap HP, 1 mL; GE Healthcare) was inserted between the gel filtration column and UV monitor. The *Sm*ChiB-containing fractions were pooled and concentrated by Microcon (Millipore) with pore size of 30 kDa, resulting in an 8.0 mg/mL *Sm*ChiB solution.

The crystallization conditions corresponded to previous work (30, 31, 40) with small modifications. Briefly, the protein solution was mixed with an equal volume of reservoir solution [0.1 M sodium phosphate, pH 7.0, 0.8 M ammonium sulfate, 5% (vol/vol) glycerol] and set up for the hanging-drop method at 298 K. The crystals of *Sm*ChiB were typically appeared in 2–3 d and grew to maximum size (~0.4 mm) in 10 d.

Preparing the *Sm*ChiB–Inhibitor Complex Crystals. We prepared the protein–inhibitor complex crystals by cocrystallization or soaking methods. We dissolved each lyophilized inhibitor and prepared inhibitor solutions as follows: *syn*-triazole (**4**) (285.8 μM in 100% methanol), azide (**2**) [5 mM in 10% (vol/vol) methanol], and 4-quinolylfromyl-*O*-allyloxime (**5**) [25 mM in 55% (vol/vol) methanol] (preparation and spectroscopic data of **5**; *SI Materials and Methods*, Figs. S1–S4). The *Sm*ChiB-azide (**2**) crystals were grown from the drop containing 1.3 μL of *Sm*ChiB solution, 0.2 μL of azide (**2**) solution, and 1.0 μL of reservoir. For soaking methods, the inhibitor solutions were added to crystallization drops where the apo-*Sm*ChiB crystals were well grown, and then sealed with vapor grease again and placed for two or three nights at 293 K. All crystals were transferred to cryoprotectant solution [0.1 M sodium phosphate, pH 7.0, 0.8 M ammonium sulfate, 20% (vol/vol) glycerol] for 10 s, and then flash-frozen and stored in liquid nitrogen until the X-ray data collection.

Data Collection, Structure Determination, and Refinement. Diffraction data were collected at AR-NW12A, AR-NE3A, BL-5A, and BL-17A in Photon Factory (Tsukuba, Japan). The crystals were diffracted to 1.7- to 2.3-Å resolution. We processed the diffraction image data with HKL-2000 (41). The crystals belonged to a tetragonal lattice with space group of $P4_32_12$, which differs from previous results (30, 31, 40). The intensity data were converted to structure factors with TRUNCATE (42), and followed by molecular replacement with MOLREP (43) using *Sm*ChiB monomer (40) as a search model. We refined the model by Refmac5 (44) and manually fixing using COOT (45). The restriction library and coordinates of inhibitors were prepared using the PRODRG2 server (http://davapc1.bioch.dundee.ac.uk/prodrg/) (46). The data collection and structure refinement statistics are summarized in *SI Text* (Table S1 and Fig. S5).

Figure Preparations. All figures for X-ray cocrystal structure were created by PyMOL (www.pymol.org), except Fig. 2*B*, which was created by LIGPLOT (47).

Computational Analysis of Huisgen Cycloaddition in *Sm*ChiB. The model structure used in our calculations consisted of **2**, **3**, and a total of 39 *Sm*ChiB residues (Tyr10, Tyr11, Phe12, Ile13, Pro14, Phe51, Ser93, Ile94, Gly95, Gly96,

Trp97, Tyr98, Asp142, Trp143, Glu144, Ala184, Phe191, Met212, Thr213, Tyr214, Asp215, Pro219, Trp220, Tyr292, Gly293, Arg294, Pro313, Gly314, Glu315, Asp316, Pro317, Asp336, Pro337, Arg338, Ile339, Met401, Phe402, Trp403, and Gln407) located within 5 Å from these two compounds. The N-terminal and C-terminal residues in our system were capped by an acetyl and *N*-methyl group, respectively. We used a total of 12 atoms, including "the azide and the contiguous methylene groups of **2**" and "propyne group of **3**" in the high QM layer. The other 887 atoms are included in the MM layer. The geometries of the precursor state, TS, and product complex were optimized at the ONIOM(B3LYP/6-31G*:AMBER) level. Subsequently, one-point energy calculations at the B3LYP/6-31G* level were carried out with the optimized structures to estimate relative energy differences. The ONIOM and B3LYP calculations were carried out using the Gaussian 03 program package (48).

ACKNOWLEDGMENTS. We thank Dr. K. Nagai and Ms. N. Sato (School of Pharmacy, Kitasato University) for various instrumental analyses and Mr. J. Kawamata (Tokushima University) for helping with the crystallization. We acknowledge the beamline staff at Photon Factory for supporting the data collection under proposals 2009G074 and 2011G135. This work was supported by a grant for the 21st Century Center of Excellence Program. This work was partly supported by Grants-in-Aid for Young Scientists (20770085) and Scientific Research (23570139) (to N.M.); as well as for Scientific Research (24590058) (to H.G.) from the Ministry of Education, Culture, Sports, Science and Technology, and a Kitasato University Research Grant for Young Researchers; and the Research Foundation for Pharmaceutical Sciences (to T.H.). The BL44XU at SPring-8 was equipped with an MX225-HE detector (Rayonix) and financially supported by the Academia Sinica and the National Synchrotron Radiation Research Center (Taiwan).

1. Huisgen R (1984) *1,3-Dipolar Cycloaddition Chemistry*, ed Padwa A (Wiley, New York), Vol 1, pp 1–176.
2. Tornøe CW, Christensen C, Meldal M (2002) Peptidotriazoles on solid phase: [1,2,3]-Triazoles by regiospecific copper(I)-catalyzed 1,3-dipolar cycloadditions of terminal alkynes to azides. *J Org Chem* 67(9):3057–3064.
3. Rostovtsev VV, Green LG, Fokin VV, Sharpless KB (2002) A stepwise Huisgen cycloaddition process: Copper(I)-catalyzed regioselective "ligation" of azides and terminal alkynes. *Angew Chem Int Ed Engl* 41(14):2596–2599.
4. Mamidyala SK, Finn MG (2010) In situ click chemistry: Probing the binding landscapes of biological molecules. *Chem Soc Rev* 39(4):1252–1261.
5. Lewis WG, et al. (2002) Click chemistry in situ: Acetylcholinesterase as a reaction vessel for the selective assembly of a femtomolar inhibitor from an array of building blocks. *Angew Chem Int Ed* 41(6):1053–1057.
6. Manetsch R, et al. (2004) In situ click chemistry: Enzyme inhibitors made to their own specifications. *J Am Chem Soc* 126(40):12809–12818.
7. Krasiński A, et al. (2005) In situ selection of lead compounds by click chemistry: Target-guided optimization of acetylcholinesterase inhibitors. *J Am Chem Soc* 127(18): 6686–6692.
8. Mocharla VP, et al. (2004) In situ click chemistry: Enzyme-generated inhibitors of carbonic anhydrase II. *Angew Chem Int Ed Engl* 44(1):116–120.
9. Whiting M, et al. (2006) Inhibitors of HIV-1 protease by using in situ click chemistry. *Angew Chem Int Ed Engl* 45(9):1435–1439.
10. Wang J, et al. (2006) Integrated microfluidics for parallel screening of an in situ click chemistry library. *Angew Chem Int Ed Engl* 45(32):5276–5281.
11. Hirose T, et al. (2009) Chitinase inhibitors: Extraction of the active framework from natural argifin and use of in situ click chemistry. *J Antibiot (Tokyo)* 62(5):277–282.
12. Wang Y, et al. (2009) An integrated microfluidic device for large-scale in situ click chemistry screening. *Lab Chip* 9(16):2281–2285.
13. Lee SS, et al. (2010) Accurate MALDI-TOF/TOF sequencing of one-bead-one-compound peptide libraries with application to the identification of multiligand protein affinity agents using in situ click chemistry screening. *Anal Chem* 82(2):672–679.
14. Willand N, et al. (2010) Exploring drug target flexibility using in situ click chemistry: Application to a mycobacterial transcriptional regulator. *ACS Chem Biol* 5(11): 1007–1013.
15. Millward SW, et al. (2011) Iterative in situ click chemistry assembles a branched capture agent and allosteric inhibitor for Akt1. *J Am Chem Soc* 133(45):18280–18288.
16. Grimster NP, et al. (2012) Generation of candidate ligands for nicotinic acetylcholine receptors via in situ click chemistry with a soluble acetylcholine binding protein template. *J Am Chem Soc* 134(15):6732–6740.
17. Deshpande MV, O'Donnell R, Gooday GW (1997) Regulation of chitin synthase activity in the dimorphic fungus *Benjaminiella poitrasii* by external osmotic pressure. *FEMS Microbiol Lett* 152(2):327–332.
18. Kuranda MJ, Robbins PW (1991) Chitinase is required for cell separation during growth of *Saccharomyces cerevisiae*. *J Biol Chem* 266(29):19758–19767.
19. Merzendorfer H, Zimoch L (2003) Chitin metabolism in insects: Structure, function and regulation of chitin synthases and chitinases. *J Exp Biol* 206(Pt 24):4393–4412.
20. Boot RG, et al. (2001) Identification of a novel acidic mammalian chitinase distinct from chitotriosidase. *J Biol Chem* 276(9):6770–6778.
21. Shahabuddin M, Toyoshima T, Aikawa M, Kaslow DC (1993) Transmission-blocking activity of a chitinase inhibitor and activation of malarial parasite chitinase by mosquito protease. *Proc Natl Acad Sci USA* 90(9):4266–4270.
22. Shibata Y, Foster LA, Bradfield JF, Myrvik QN (2000) Oral administration of chitin down-regulates serum IgE levels and lung eosinophilia in the allergic mouse. *J Immunol* 164(3):1314–1321.
23. Henrissat B, Bairoch A (1993) New families in the classification of glycosyl hydrolases based on amino acid sequence similarities. *Biochem J* 293(Pt 3):781–788.
24. Terwisscha van Scheltinga AC, Hennig M, Dijkstra BW (1996) The 1.8 A resolution structure of hevamine, a plant chitinase/lysozyme, and analysis of the conserved sequence and structure motifs of glycosyl hydrolase family 18. *J Mol Biol* 262(2): 243–257.
25. Gloeckner C, et al. (2010) Repositioning of an existing drug for the neglected tropical disease Onchocerciasis. *Proc Natl Acad Sci USA* 107(8):3424–3429.
26. Arai N, et al. (2000) Argadin, a new chitinase inhibitor, produced by *Clonostachys* sp. FO-7314. *Chem Pharm Bull (Tokyo)* 48(10):1442–1446.
27. Ōmura S, et al. (2000) Argifin, a new chitinase inhibitor, produced by *Gliocladium* sp. FTD-0668. I. Taxonomy, fermentation, and biological activities. *J Antibiot (Tokyo)* 53(6):603–608.
28. Arai N, Shiomi K, Iwai Y, Ōmura S (2000) Argifin, a new chitinase inhibitor, produced by *Gliocladium* sp. FTD-0668. II. Isolation, physico-chemical properties, and structure elucidation. *J Antibiot (Tokyo)* 53(6):609–614.
29. Shiomi K, et al. (2000) Structure of argifin, a new chitinase inhibitor produced by *Gliocladium* sp. *Tetrahedron Lett* 41(13):2141–2143.
30. van Aalten DMF, et al. (2001) Structural insights into the catalytic mechanism of a family 18 exo-chitinase. *Proc Natl Acad Sci USA* 98(16):8979–8984.
31. Houston DR, et al. (2002) High-resolution structures of a chitinase complexed with natural product cyclopentapeptide inhibitors: Mimicry of carbohydrate substrate. *Proc Natl Acad Sci USA* 99(14):9127–9132.
32. Rao FV, et al. (2005) Specificity and affinity of natural product cyclopentapeptide inhibitors against *A. fumigatus*, human, and bacterial chitinases. *Chem Biol* 12(1): 65–76.
33. Andersen OA, Nathubhai A, Dixon MJ, Eggleston IM, van Aalten DMF (2008) Structure-based dissection of the natural product cyclopentapeptide chitinase inhibitor argifin. *Chem Biol* 15(3):295–301.
34. Bourne Y, et al. (2004) Freeze-frame inhibitor captures acetylcholinesterase in a unique conformation. *Proc Natl Acad Sci USA* 101(6):1449–1454.
35. Case DA, et al. (2006) AMBER 9 (Univ of California, San Francisco).
36. Cornell WD, et al. (1995) A second generation force field for the simulation of proteins, nucleic acids, and organic molecules. *J Am Chem Soc* 117(19):5179–5197.
37. Dapprich S, Komáromi I, Byun KS, Morokuma K, Frisch MJ (1999) A new ONIOM implementation in Gaussian 98. Part 1. The calculation of energies, gradients and vibrational frequencies and electric field derivatives. *J Mol Struct THEOCHEM* 461–462: 1–21.
38. Vreven T, Morokuma K, Farkas Ö, Schlegel HB, Frisch MJ (2003) Geometry optimization with QM/MM, ONIOM, and other combined methods. I. Microiterations and constraints. *J Comput Chem* 24(6):760–769.
39. Himo F, et al. (2005) Copper(I)-catalyzed synthesis of azoles. DFT study predicts unprecedented reactivity and intermediates. *J Am Chem Soc* 127(1):210–216.
40. van Aalten DMF, et al. (2000) Structure of a two-domain chitotriosidase from *Serratia marcescens* at 1.9-A resolution. *Proc Natl Acad Sci USA* 97(11):5842–5847.
41. Otwinowski Z, Minor W (1997) Processing of X-ray diffraction data collected in oscillation mode. *Methods Enzymol* 276:307–326.
42. Winn MD, et al. (2011) Overview of the CCP4 suite and current developments. *Acta Crystallogr D Biol Crystallogr* 67(Pt 4):235–242.
43. Vagin A, Teplyakov A (2010) Molecular replacement with MOLREP. *Acta Crystallogr D Biol Crystallogr* 66(Pt 1):22–25.
44. Murshudov GN, et al. (2011) REFMAC5 for the refinement of macromolecular crystal structures. *Acta Crystallogr D Biol Crystallogr* 67(Pt 4):355–367.
45. Emsley P, Lohkamp B, Scott WG, Cowtan K (2010) Features and development of Coot. *Acta Crystallogr D Biol Crystallogr* 66(Pt 4):486–501.
46. Schüttelkopf AW, van Aalten DMF (2004) PRODRG: A tool for high-throughput crystallography of protein-ligand complexes. *Acta Crystallogr D Biol Crystallogr* 60(Pt 8):1355–1363.
47. Wallace AC, Laskowski RA, Thornton JM (1995) LIGPLOT: A program to generate schematic diagrams of protein-ligand interactions. *Protein Eng* 8(2):127–134.
48. Frisch MJ, et al. (2004) Gaussian 03 (Gaussian, Wallingford, CT).